ELSEVIER

International Journal of Solids and Structures 41 (2004) 2659–2683

INTERNATIONAL JOURNAL OF SOLIDS and STRUCTURES

www.elsevier.com/locate/ijsolstr

Effect of elastic matrix constraint on the tensile deformation of NiTi superelastic fiber

Xiang-Bin Yu [a,b], Qing-Ping Sun [a,*], Zheng Zhong [b]

[a] *Department of Mechanical Engineering, The Hong Kong University of Science and Technology, Clear Water Bay, Kowloon, Hong Kong SAR, PR China*

[b] *Solid Mechanics Key Laboratory of MOE, Department of Engineering Mechanics and Technology, Tongji University, Shanghai 200092, PR China*

Received 6 March 2003; received in revised form 17 November 2003

Abstract

In this paper we study the effect of elastic matrix constraint on the tensile deformation of an active NiTi shape memory alloy fiber, which, when no matrix constraint is present, will experience stress-induced phase transformation by nucleation and growth of a macroscopic martensite band. The effect of the constraint is measured by two factors: the relative Young's modulus (by dimensionless parameter $E^{(2)}/E^{(1)}$) and the relative dimension (by dimensionless parameter h/a) of the fiber and the matrix. The transformation process of the fiber through the martensite band growth under tension is modeled as an embedded elastic fiber containing growing cylindrical transformation inclusions. By Love's stress function, the elastic solutions of the inclusion–fiber–matrix system as well as the internal elastic energy during the transformation are obtained. Analytical expressions of the free energy of the system during the transformation are also formulated for the case of uniaxial tension. After introducing the band nucleation and growth criteria, the growth capability of a martensite band is examined. The results demonstrate that, depending on the magnitude of the matrix constraint, three distinct deformation patterns of the fiber exist: (1) with weak matrix constraint, single band growth dominates the transformation process of the fiber; (2) with intermediate matrix constraint, sequential bands nucleation and growth prevails in the fiber; and (3) with strong constraint, numerous bands form and grow, and macroscopically the fiber tends to deform homogeneously. Parametric studies on the macroscopic stress–strain response of the fiber–matrix system are performed and the obtained results are discussed.

Keywords: Uniaxial tension; NiTi superelastic shape memory alloy fiber; Phase transition; Matrix constraint; Deformation instability; Deformation patterns

* Corresponding author. Tel.: +852-23588655; fax: +852-23581543.
E-mail address: meqpsun@ust.hk (Q.-P. Sun).

0020-7683/$ - see front matter © 2003 Elsevier Ltd. All rights reserved.
doi:10.1016/j.ijsolstr.2003.12.004

1. Introduction

In the last decade, intensive research has been done on the deformation of thermoelastic solids undergoing martensitic phase transition (such as NiTi polycrystalline superelastic shape memory alloy (SMA) fibers, strips and tubes under tension). Systematic experiments (e.g., Shaw and Kyriakides, 1995; Miyazaki et al., 1982) demonstrated that the deformation of a NiTi superelastic fiber or strip is realized by the nucleation and propagation of one or several transformation bands, similar to the Luders bands phenomenon in mild steels. The intrinsic mechanisms underpinning this inhomogeneous deformation, though known in certain degree, are still being investigated. One of the explanations is that macroscopic constitutive relation of the material exhibits a kind of strain softening (during transformation) and rehardening (after exhaust of transformation) in a so-called up-down-up nonlinear fashion as first introduced by Ericken (1975). In the theoretical aspect, considerable efforts have been devoted to the study of such constitutive relations and related structure responses. Significant progress has been achieved in understanding and modeling the behaviors of materials during phase transition (e.g., Triantafyllidis and Bardenhagen, 1993; Abeyaratne and Knowles, 1990, 1993; Coleman, 1983).

Parallel to the above fundamental research, Cu- and Ni-based shape memory alloys have been successfully embedded in elastic or elastoplastic matrix as the active elements in composite materials and also in conventional structures to achieve certain control, sensing or actuating functions (e.g., Furuya, 1996; Duerig and Melton, 1989). Typical configurations are SMA products with different surface coatings and composites reinforced with shape memory alloy fibers. In such applications, it is important to understand how matrix constraints influence the deformation of a fiber that would experience deformation instability had it not been under the matrix constraint. Such knowledge will benefit the development of composite materials since matrix constraint could have an effect on fiber transformation, which in turn affects the internal stress state of the composite. So far, quantitative mechanical modeling and a clear picture of the transformation process in active SMA fibers under various matrix constraints are not available in the literature.

To our knowledge, there are two analytical approaches for studying the mechanics of fiber–matrix system under external loading. The first is based on given constitutive relations of the fiber and matrix introduced. Along this line, there have been micromechanics models for SMA composite (Song et al., 1999; Cherkaoui et al., 2000), one-dimensional (1-D) analysis on layered adaptive composites (Roytburd and Slutsker, 1999a,b, 2001) and the deformation analysis of active materials laid on an elastic foundation (Truskinovsky and Zanzotto, 1995, 1996). However, analytical solutions for 2-D and 3-D problems are very complicated mathematically and have not been reported in the literature. The second approach to handle the problem is to assume the geometry of the martensite domain or deformation patterns (Tsai and Fan, 2002; Sun and Zhong, 2000; Zhong et al., 2000) and carry out the analysis under certain geometric assumptions. This approach has several advantages in dealing with a particular type of experimentally observed geometry of deformation patterns, even though, as pointed out by James (1990), it suffers from a number of severe limitations (for example, the assumed location of the phase interface may not be energy minimized).

The present study adopts the second approach to analyze the deformation of the fiber–matrix system. Instead of introducing the nonlinear constitutive equations of the active NiTi fiber, we quantify the martensite domain as an elastic transformation inclusion problem. Such simplification is due partially to experimental observations and empirical assumptions and partially to our intention to make the problem mathematically tractable. Using this approach, we attempt to clarify and answer the following questions:

(1) If a band is nucleated in the constrained fiber, what are the stress state and energetic features of the fiber–matrix system containing this band?

(2) What is the growth ability of this nucleated band or the mobility of the prescribed interface with further loading and how this depends on the matrix constraint?
(3) What are the possible deformation patterns of the constrained fiber and the corresponding macroscopic stress strain responses of the fiber–matrix system during loading?

This paper is organized as follows. In Section 2, the problem investigated is described and formulated. We assume a pre-existing band in the active fiber and simulate the fiber as an elastic rod containing a single growing cylindrical transformation inclusion with uniform axisymmetric transformation strain. In Section 3, the analytical expressions of the stress and strain of the inclusion–fiber–matrix (IFM) system are obtained by the principle of superposition and Love's stress function (Timoshenko and Goodier, 1951). Based on the stress solution, the energetics of the system is calculated in Section 4. The driving force and the condition for the quasi-static growth of this existing band are derived. In Section 5, we first give the overall responses of the system for the case of a single band growth process. After introducing the band nucleation criteria, the growth ability of a band or the mobility of the interface is examined. Depending on the magnitude of the constraint, distinct transformation processes and the corresponding deformation patterns of the fiber are identified. The obtained macroscopic responses of the system as well as the energetic features are finally discussed in Section 6.

It must be noted that in general the stress-induced transformation of SMA should be treated as a time-dependent process with thermomechanical coupling. In this paper, the heat effect is neglected. We focus solely on the mechanical aspect of the isothermal and quasi-static case, which might be a good approximation for the IFM system under slow loading rates.

2. Problem statement, basic assumptions and governing equations

Consider a long NiTi superelastic fiber with a circular cross section of radius a wrapped by an elastic matrix of thickness h (Fig. 1). The interface between the fiber and matrix is perfect that the traction and displacement across it are continuous. During phase transformation induced by the applied load, the constrained fiber will evolve into a mixture of Austenite and Martensite phases. To make the problem tractable, we assume that the martensite in the fiber takes the shape of a cylindrical inclusion with interfaces perpendicular to the loading axis (z axis). The parameter l denotes the length of the inclusion as shown in Fig. 1. For simplicity, we further assume that the modulus of the martensite and austenite are the same (for the case of distinct elastic moduli of the two phases, see Stupkiewicz and Petryk, 2002). The transformation strain inside the band is uniform and axisymmetric with respect to z axis. With the above assumptions, the transformation process of the constrained fiber under tension can be modeled by the nucleation and growth process of the inclusion.

To analyze the above IFM system, a cylindrical coordinate system (r, θ, z) is used, with the z axis being placed along the revolutionary axis of the cylinder. The nonzero components of the axisymmetric eigenstrain ε^* uniformly distributed in the inclusion can be written as

$$\varepsilon_r^* = \varepsilon_\theta^* = \varepsilon_1^* \quad \varepsilon_z^* = \varepsilon_2^* \tag{1}$$

In cylindrical coordinates, the corresponding displacement components are $u_r^{(1)}$, $u_\theta^{(1)}$, and $u_z^{(1)}$ in the matrix and $u_r^{(2)}$, $u_\theta^{(2)}$ and $u_z^{(2)}$ in the fiber. Throughout this paper, superscripts 1 and 2 will be used to denote the quantities of the matrix and the fiber respectively. Because of the axisymmetric nature of the problem, the components $u_\theta^{(i)}$ $(i = 1, 2)$ vanish and $u_r^{(i)}$, $u_z^{(i)}$ $(i = 1, 2)$ are independent of θ. The nonzero strain components are $\varepsilon_r^{(i)}$, $\varepsilon_\theta^{(i)}$, $\varepsilon_z^{(i)}$, $\gamma_{rz}^{(i)}$ $(i = 1, 2)$ and the nonzero stress components are $\sigma_r^{(i)}$, $\sigma_\theta^{(i)}$, $\sigma_z^{(i)}$, $\tau_{rz}^{(i)}$ $(i = 1, 2)$.

The Governing equations and boundary conditions needed to obtain the above elastic fields of an infinite long domain are as follows.

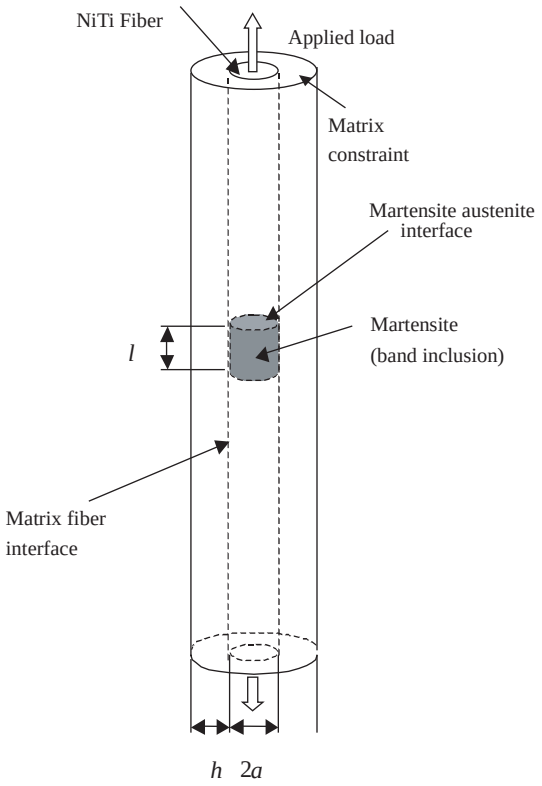

Fig. 1. A schematic presentation of an IFM system, in which a superelastic NiTi fiber is embedded in an elastic matrix and has been transformed into a mixture of martensite and austenite phases under external tensile load.

Kinematical equations:

$$\varepsilon_r^{(i)} = \frac{\partial u_r^{(i)}}{\partial r}, \quad \varepsilon_\theta^{(i)} = \frac{u_r^{(i)}}{r}, \quad \varepsilon_z^{(i)} = \frac{\partial u_z^{(i)}}{\partial z}, \quad \gamma_{rz}^{(i)} = \frac{\partial u_r^{(i)}}{\partial z} + \frac{\partial u_z^{(i)}}{\partial r} \quad (i = 1, 2) \tag{2}$$

Constitutive equations:

For stress components in the inclusion $|z| < l/2$, $r < a$, we have

$$\begin{aligned}
\sigma_r^{(2)} &= \frac{E^{(2)}}{1+v^{(2)}}\left[\frac{v^{(2)}}{1-2v^{(2)}}(\theta^{(2)} - \theta^*) + (\varepsilon_r^{(2)} - \varepsilon_r^*)\right] \\
\sigma_\theta^{(2)} &= \frac{E^{(2)}}{1+v^{(2)}}\left[\frac{v^{(2)}}{1-2v^{(2)}}(\theta^{(2)} - \theta^*) + (\varepsilon_\theta^{(2)} - \varepsilon_\theta^*)\right] \\
\sigma_z^{(2)} &= \frac{E^{(2)}}{1+v^{(2)}}\left[\frac{v^{(2)}}{1-2v^{(2)}}(\theta^{(2)} - \theta^*) + (\varepsilon_z^{(2)} - \varepsilon_z^*)\right] \\
\tau_{rz}^{(2)} &= \frac{E^{(2)}}{2(1+v^{(2)})}\gamma_{rz}^{(2)}
\end{aligned} \tag{3}$$

For stress in the other regions

$$\begin{aligned}
\sigma_r^{(i)} &= \frac{E^{(i)}}{1+v^{(i)}}\left[\frac{v^{(i)}}{1-2v^{(i)}}\theta^{(i)} + \varepsilon_r^{(i)}\right] \\
\sigma_\theta^{(i)} &= \frac{E^{(i)}}{1+v^{(i)}}\left[\frac{v^{(i)}}{1-2v^{(i)}}\theta^{(i)} + \varepsilon_\theta^{(i)}\right] \\
\sigma_z^{(i)} &= \frac{E^{(i)}}{1+v^{(i)}}\left[\frac{v^{(i)}}{1-2v^{(i)}}\theta^{(i)} + \varepsilon_z^{(i)}\right] \\
\tau_{rz}^{(i)} &= \frac{E^{(i)}}{2(1+v^{(i)})}\gamma_{rz}^{(i)}
\end{aligned} \quad (i=1,2) \tag{4}$$

where $E^{(i)}$, $v^{(i)}$ are Young's moduli and Poisson's ratio, and $\theta^{(i)} = \varepsilon_r^{(i)} + \varepsilon_\theta^{(i)} + \varepsilon_z^{(i)}$, $\theta^* = \varepsilon_r^* + \varepsilon_\theta^* + \varepsilon_z^*$.

Equation of equilibrium:

$$\begin{aligned}
&\frac{\partial\sigma_r^{(i)}}{\partial r} + \frac{\partial\tau_{rz}^{(i)}}{\partial z} + \frac{\sigma_r^{(i)} - \sigma_\theta^{(i)}}{r} = 0 \\
&\frac{\partial\tau_{rz}^{(i)}}{\partial r} + \frac{\partial\sigma_z^{(i)}}{\partial z} + \frac{\tau_{rz}^{(i)}}{r} = 0
\end{aligned} \tag{5}$$

Boundary conditions:

Stress-free condition of the outer surface requires

$$\sigma_r^{(1)} = \tau_{rz}^{(1)} = 0 \quad (r = a+h) \tag{6}$$

The continuity of traction and displacement across the wire and matrix interface requires

$$\begin{aligned}
&\sigma_r^{(1)} = \sigma_r^{(2)} \quad (r=a) \\
&\tau_{rz}^{(1)} = \tau_{rz}^{(2)} \quad (r=a) \\
&u_r^{(1)} = u_r^{(2)} \quad (r=a) \\
&u_z^{(1)} = u_z^{(2)} \quad (r=a)
\end{aligned} \tag{7}$$

And at the infinity

$$\sigma_r^{(i)} = \sigma_\theta^{(i)} = \sigma_z^{(i)} = \tau_{rz}^{(i)} = 0 \quad (|z| \to \infty)\ (i=1,2) \tag{8}$$

In the next section, the internal stress and strain energy induced in this infinite domain by this single inclusion will be determined. It will play a central role in the evolution of the finite long fiber matrix system.

3. Solution of the single inclusion problem

Under small strain condition, the original single inclusion problem of Fig. 1 can be decomposed into three sub-problems as schemed in Fig. 2. In sub-problem I, the matrix deforms under the radial stress and shear stress prescribed on the inner surface. In sub-problem II the NiTi fiber deforms under the radial stress and shear stress prescribed on the outer surface, which have the same magnitude but opposite directions as those in sub-problem I. In sub-problem III the NiTi fiber deforms due to the inclusion without any other prescribed constraint.

In the following parts, superscripts "I", "II" and "III" are used to denote quantities of sub-problem "I", "II" and "III" respectively (Note: superscripts ($i = 1, 2$) used to indicate quantities belonging to matrix or fiber are encompassed by parentheses).

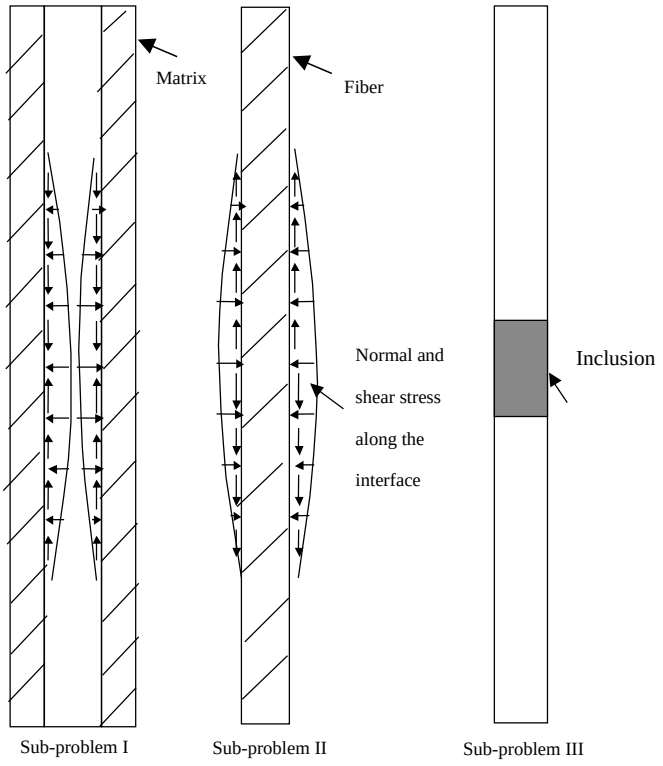

Fig. 2. A schematic presentation of the decomposition of the original single inclusion problem into three sub-problems.

3.1. Solutions of sub-problem I and II

A standard way to solve axisymmetric elastic problem is to employ Love's stress functions ϕ. The stress and displacement components expressed by ϕ are

$$\begin{aligned}
\sigma_r &= \frac{\partial}{\partial z}\left(v\nabla^2\phi - \frac{\partial^2\phi}{\partial r^2}\right),\\
\sigma_\theta &= \frac{\partial}{\partial z}\left(v\nabla^2\phi - \frac{1}{r}\frac{\partial\phi}{\partial r}\right),\\
\sigma_z &= \frac{\partial}{\partial z}\left[(2-v)\nabla^2\phi - \frac{\partial^2\phi}{\partial r^2}\right],\\
\tau_{rz} &= \frac{\partial}{\partial r}\left[(1-v)\nabla^2\phi - \frac{\partial^2\phi}{\partial z^2}\right],\\
u_r &= -\frac{1+v}{E}\frac{\partial^2\phi}{\partial r\partial z},\\
u_z &= \frac{1+v}{E}\left[2(1-v)\nabla^2\phi - \frac{\partial^2\phi}{\partial z^2}\right],
\end{aligned} \tag{9}$$

where E and v are respectively Young's modulus and Poisson's ratio of the isotropic material considered. The equilibrium equation are satisfied provided that ϕ satisfies bi-harmonic equation

$$\nabla^2\nabla^2\phi = 0 \tag{10}$$

In order to satisfy the bi-harmonic equation and boundary condition, in solving sub-problem I, the stress function is assumed as

$$\phi^{\mathrm{I}} = 2\int_0^\infty [-\rho_1^{\mathrm{I}}(k)krI_1(kr) + \rho_2^{\mathrm{I}}(k)krK_1(kr) + \rho_3^{\mathrm{I}}(k)I_0(kr) + \rho_4^{\mathrm{I}}(k)K_0(kr)]\sin(kz)\sin\left(\frac{kl}{2}\right)\mathrm{d}k \tag{11}$$

where $I_0(ka)$, $I_1(ka)$ are first-kind modified Bessel function of zero order and first order, and $K_0(ka)$, $K_1(ka)$ are second-kind modified Bessel function of zero order and first order. The unknown functions ρ_1^{I}, ρ_2^{I}, ρ_3^{I}, ρ_4^{I} will be determined later by the boundary conditions. Substituting Eq. (11) into Eq. (9), we obtain the stress and displacement components of the sub-problem I:

$$\tau_{rz}^{\mathrm{I}} = 2\int_0^\infty [\rho_1^{\mathrm{I}}(k)M_{11}(kr) + \rho_2^{\mathrm{I}}(k)M_{12}(kr) + \rho_3^{\mathrm{I}}(k)M_{13}(kr) + \rho_4^{\mathrm{I}}(k)M_{14}(kr)]k^3\sin(kz)\sin\left(\frac{kl}{2}\right)\mathrm{d}k \tag{12.1}$$

$$\sigma_r^{\mathrm{I}} = 2\int_0^\infty [\rho_1^{\mathrm{I}}(k)M_{21}(kr) + \rho_2^{\mathrm{I}}(k)M_{22}(kr) + \rho_3^{\mathrm{I}}(k)M_{23}(kr) + \rho_4^{\mathrm{I}}(k)M_{24}(kr)]k^3\cos(kz)\sin\left(\frac{kl}{2}\right)\mathrm{d}k \tag{12.2}$$

$$\sigma_z^{\mathrm{I}} = 2\int_0^\infty [\rho_1^{\mathrm{I}}(k)M_{31}(kr) + \rho_2^{\mathrm{I}}(k)M_{32}(kr) + \rho_3^{\mathrm{I}}(k)M_{33}(kr) + \rho_4^{\mathrm{I}}(k)M_{34}(kr)]k^3\cos(kz)\sin\left(\frac{kl}{2}\right)\mathrm{d}k \tag{12.3}$$

$$\sigma_\theta^{\mathrm{I}} = 2\int_0^\infty [\rho_1^{\mathrm{I}}(k)M_{41}(kr) + \rho_2^{\mathrm{I}}(k)M_{42}(kr) + \rho_3^{\mathrm{I}}(k)M_{43}(kr) + \rho_4^{\mathrm{I}}(k)M_{44}(kr)]k^3\cos(kz)\sin\left(\frac{kl}{2}\right)\mathrm{d}k \tag{12.4}$$

$$u_r^{\mathrm{I}} = \frac{2(1+v^{(1)})}{E^{(1)}}\int_0^\infty [\rho_1^{\mathrm{I}}(k)\chi_{11}(kr) + \rho_2^{\mathrm{I}}(k)\chi_{12}(kr) + \rho_3^{\mathrm{I}}(k)\chi_{13}(kr) + \rho_4^{\mathrm{I}}(k)\chi_{14}(kr)]k^2\cos(kz)\sin\left(\frac{kl}{2}\right)\mathrm{d}k \tag{12.5}$$

$$u_z^{\mathrm{I}} = \frac{2(1+v^{(1)})}{E^{(1)}}\int_0^\infty [\rho_1^{\mathrm{I}}(k)\chi_{21}(kr) + \rho_2^{\mathrm{I}}(k)\chi_{22}(kr) + \rho_3^{\mathrm{I}}(k)\chi_{23}(kr) + \rho_4^{\mathrm{I}}(k)\chi_{24}(kr)]k^2\sin(kz)\sin\left(\frac{kl}{2}\right)\mathrm{d}k \tag{12.6}$$

The expressions of M_{ij} and χ_{ij} in these equations are listed in Appendix A.

For sub-problem II, the stress function ϕ^{II} is assumed as

$$\phi^{\mathrm{II}} = 2\int_0^\infty [-\rho_1^{\mathrm{II}}(k)krI_1(kr) + \rho_3^{\mathrm{II}}(k)I_0(kr)]\sin(kz)\sin\left(\frac{kl}{2}\right)\mathrm{d}k \tag{13}$$

where ρ_1^{II}, ρ_3^{II} are unknown functions. The corresponding stress and displacement components in the fiber are obtained as

$$\tau_{rz}^{\mathrm{II}} = 2\int_0^\infty [\rho_1^{\mathrm{II}}(k)M_{11}(kr) + \rho_3^{\mathrm{II}}(k)M_{13}(kr)]k^3\sin(kz)\sin\left(\frac{kl}{2}\right)\mathrm{d}k \tag{14.1}$$

$$\sigma_r^{\mathrm{II}} = 2\int_0^\infty [\rho_1^{\mathrm{II}}(k)M_{21}(kr) + \rho_3^{\mathrm{II}}(k)M_{23}(kr)]k^3\cos(kz)\sin\left(\frac{kl}{2}\right)\mathrm{d}k \tag{14.2}$$

$$\sigma_z^{\mathrm{II}} = 2\int_0^\infty [\rho_1^{\mathrm{II}}(k)M_{31}(kr) + \rho_3^{\mathrm{II}}(k)M_{33}(kr)]k^3\cos(kz)\sin\left(\frac{kl}{2}\right)\mathrm{d}k \tag{14.3}$$

$$\sigma_\theta^{\mathrm{II}} = 2\int_0^\infty [\rho_1^{\mathrm{II}}(k)M_{41}(kr) + \rho_3^{\mathrm{II}}(k)M_{43}(kr)]k^3\cos(kz)\sin\left(\frac{kl}{2}\right)\mathrm{d}k \tag{14.4}$$

$$u_r^{\mathrm{II}} = \frac{2(1+v^{(2)})}{E^{(2)}}\int_0^\infty [\rho_1^{\mathrm{II}}(k)\chi_{11}(kr) + \rho_3^{\mathrm{II}}(k)\chi_{13}(kr)]k^2\cos(kz)\sin\left(\frac{kl}{2}\right)\mathrm{d}k \tag{14.5}$$

$$u_z^{\mathrm{II}} = \frac{2(1+v^{(2)})}{E^{(2)}}\int_0^\infty [\rho_1^{\mathrm{II}}(k)\chi_{21}(kr) + \rho_3^{\mathrm{II}}(k)\chi_{23}(kr)]k^2\sin(kz)\sin\left(\frac{kl}{2}\right)\mathrm{d}k \tag{14.6}$$

3.2. Solution of sub-problem III

The solution of sub-problem III is available in literature (Zhong et al., 2000). The results are summarized below:

$$\tau_{rz}^{\mathrm{III}} = 2\int_0^\infty \{[\rho(k) - 2(1-v^{(2)})]I_1(kr) - krI_0(kr)\}k^3 f(k)\sin(kz)\sin\left(\frac{kl}{2}\right)\mathrm{d}k \tag{15.1}$$

$$\begin{cases} \sigma_r^{\mathrm{III}} = 2\int_0^\infty \left\{[1-2v^{(2)}-\rho(k)]I_0(kr) + \left[kr + \frac{\rho(k)}{kr}\right]I_1(kr)\right\}k^3 f(k)\cos(kz)\sin\left(\frac{kl}{2}\right)\mathrm{d}k - \frac{E^{(2)}}{1-v^{(2)}}\varepsilon_1^* & |z| < \frac{l}{2} \\ \sigma_r^{\mathrm{III}} = 2\int_0^\infty \left\{[1-2v^{(2)}-\rho(k)]I_0(kr) + \left[kr + \frac{\rho(k)}{kr}\right]I_1(kr)\right\}k^3 f(k)\cos(kz)\sin\left(\frac{kl}{2}\right)\mathrm{d}k & |z| > \frac{l}{2} \end{cases} \tag{15.2}$$

$$\sigma_z^{\mathrm{III}} = 2\int_0^\infty \{[\rho(k) - 2(2-v^{(2)})]I_0(kr) - krI_1(kr)\}k^3 f(k)\cos(kz)\sin\left(\frac{kl}{2}\right)\mathrm{d}k \tag{15.3}$$

$$\begin{cases} \sigma_\theta^{\mathrm{III}} = 2\int_0^\infty \left[(1-2v^{(2)})I_0(kr) - \frac{\rho(k)}{kr}I_1(kr)\right]k^3 f(k)\cos(kz)\sin\left(\frac{kl}{2}\right)\mathrm{d}k - \frac{E^{(2)}}{1-v^{(2)}}\varepsilon_1^* & |z| < \frac{l}{2} \\ \sigma_\theta^{\mathrm{III}} = 2\int_0^\infty \left[(1-2v^{(2)})I_0(kr) - \frac{\rho(k)}{kr}I_1(kr)\right]k^3 f(k)\cos(kz)\sin\left(\frac{kl}{2}\right)\mathrm{d}k & |z| > \frac{l}{2} \end{cases} \tag{15.4}$$

$$u_r^{\mathrm{III}} = \frac{2(1+v^{(2)})}{E^{(2)}}\int_0^\infty [krI_0(kr) - \rho(k)I_1(kr)]k^2 f(k)\cos(kz)\sin\left(\frac{kl}{2}\right)\mathrm{d}k \tag{15.5}$$

$$\begin{cases} u_z^{\mathrm{III}} = \frac{2(1+v^{(2)})}{E^{(2)}}\int_0^\infty \{[\rho(k) - 4(1-v^{(2)})]I_0(kr) - krI_1(kr)\}k^2 f(k)\sin(kz)\sin\left(\frac{kl}{2}\right)\mathrm{d}k + Az & |z| < \frac{l}{2} \\ u_z^{\mathrm{III}} = \frac{2(1+v^{(2)})}{E^{(2)}}\int_0^\infty \{[\rho(k) - 4(1-v^{(2)})]I_0(kr) - krI_1(kr)\}k^2 f(k)\sin(kz)\sin\left(\frac{kl}{2}\right)\mathrm{d}k - A\frac{l}{2} & z < -\frac{l}{2} \\ u_z^{\mathrm{III}} = \frac{2(1+v^{(2)})}{E^{(2)}}\int_0^\infty \{[\rho(k) - 4(1-v^{(2)})]I_0(kr) - krI_1(kr)\}k^2 f(k)\sin(kz)\sin\left(\frac{kl}{2}\right)\mathrm{d}k + A\frac{l}{2} & z > \frac{l}{2} \end{cases} \tag{15.6}$$

where

$$\rho(k) = 2(1-v^{(2)}) + ka\frac{I_0(ka)}{I_1(ka)} \tag{16}$$

$$f(k) = -\frac{p}{\pi k^4}\left\{[1-2v^{(2)}-\rho(k)]I_0(ka) + \left[ka + \frac{\rho(k)}{ka}\right]I_1(ka)\right\}^{-1} \tag{17}$$

$$p = -\frac{E^{(2)}}{1-v^{(2)}}\varepsilon_1^*, \quad A = \frac{2v^{(2)}}{1-2v^{(2)}}\varepsilon_1^* + \varepsilon_2^* \tag{18}$$

3.3. Determination of the unknown functions

The total stress and displacement in the matrix and the fiber now can be easily obtained by superposition and expressed as

$$\begin{aligned}
&\sigma_r^{(1)} = \sigma_r^{\mathrm{I}} \qquad \tau_{rz}^{(1)} = \tau_{rz}^{\mathrm{I}} \\
&u_r^{(1)} = u_r^{\mathrm{I}} \qquad u_z^{(1)} = u_z^{\mathrm{I}} \\
&\sigma_r^{(2)} = \sigma_r^{\mathrm{II}} + \sigma_r^{\mathrm{III}} \qquad \tau_{rz}^{(2)} = \tau_{rz}^{\mathrm{II}} + \tau_{rz}^{\mathrm{III}} \\
&u_r^{(2)} = u_r^{\mathrm{II}} + u_r^{\mathrm{III}} \qquad u_z^{(2)} = u_z^{\mathrm{II}} + u_z^{\mathrm{III}}
\end{aligned} \tag{19}$$

Now the six boundary conditions in Eqs. (6) and (7) are used to determine the six unknown functions ρ_1^{I}, ρ_2^{I}, ρ_3^{I}, ρ_4^{I}, ρ_1^{II} and ρ_3^{II} in Love's stress functions. Therefore, a closed solution of the original single inclusion problem has been established. The explicit expressions of ρ_1^{I}, ρ_2^{I}, ρ_3^{I}, ρ_4^{I}, ρ_1^{II} and ρ_3^{II} can be obtained by solving these six linear equations. The approach is standard and routine (see Appendix B for details).

4. Energetics of the IFM system during phase transformation

4.1. Elastic strain energy of IFM system

As we have pointed out, the elastic strain energy W induced by the martensite inclusion plays an important role in the evolution of the IFM system. W can be calculated as (Mura, 1987)

$$W = \frac{1}{2}\int_{R^{(1)}} \sigma_{ij}^{(1)} e_{ij}^{(1)}\,\mathrm{d}V + \frac{1}{2}\int_{R^{(2)}} \sigma_{ij}^{(2)} e_{ij}^{(2)}\,\mathrm{d}V \tag{20}$$

where $R^{(1)}$ and $R^{(2)}$ indicate the regions of the matrix and fiber respectively and $e_{ij}^{(i)}$ is the elastic strain. From the continuity of the tractions and displacements across the fiber and matrix interface, the stress-free boundary condition of the outer surface of the matrix and the divergence theorem, Eq. (20) can be further simplified as

$$W = -\frac{1}{2}\int_{\Omega} \sigma_{ij}^{(2)} \varepsilon_{ij}^{*}\,\mathrm{d}V \tag{21}$$

where Ω is the domain of the inclusion (martensite phase). Substituting Eqs. (14) and (15) into (21), we get

$$W = W_1 + W_2, \tag{22}$$

where

$$W_1 = \frac{\pi a^2 l}{1 - v^{(2)}} E^{(2)} (\varepsilon_1^*)^2 H\left(\frac{l}{a}, v^{(2)}\right) \tag{23}$$

$$H\left(\frac{l}{a}, v^{(2)}\right) = 1 + \frac{a}{l}\int_0^{\infty} G(t, v^{(2)}) \left[\sin\left(\frac{tl}{2a}\right)\right]^2 \mathrm{d}t \tag{24}$$

$$G(t, v^{(2)}) = \frac{8(1 + v^{(2)})}{\pi t^3} \left\{ [1 - 2v^{(2)} - \rho(t)] \frac{I_0(t)}{I_1(t)} + t + \frac{\rho(t)}{t} \right\}^{-1} \tag{25}$$

$$\rho(t) = 2(1 - v^{(2)}) + t\frac{I_0(t)}{I_1(t)} \tag{26}$$

$$W_2 = -4\pi\varepsilon_1^* \int_0^\infty \{[2(1-2v^{(2)})\rho_1^{\mathrm{II}} - \rho_3^{\mathrm{II}}]kaI_1(ka) + k^2a^2\rho_1^{\mathrm{II}}I_2(ka)\}\left[\sin\left(\frac{kl}{2}\right)\right]^2 \mathrm{d}k$$

$$- 4\pi\varepsilon_2^* \int_0^\infty \{[-(4-2v^{(2)})\rho_1^{\mathrm{II}} + \rho_3^{\mathrm{II}}]kaI_1(ka) - k^2a^2\rho_1^{\mathrm{II}}I_2(ka)\}\left[\sin\left(\frac{kl}{2}\right)\right]^2 \mathrm{d}k \tag{27}$$

We see that the elastic strain energy W is composed of two parts: W_1 is the elastic energy of a single free fiber containing the inclusion, and W_2 is the additional energy caused by the matrix constraint. The variation of the normalized elastic strain energy $W^*(= W/a^3E^{(2)}(\varepsilon_1^*)^2)$ versus the normalized length of inclusion l/a is shown in Figs. 3–5, from which the following features can be identified:

(1) For a fiber without matrix constraint (Fig. 3), this strain energy first increases steeply with l and quickly reaches a peak value ($l/a \approx 0.6$), it then decreases with further growth of the martensite inclusion and finally asymptotically reaches its steady-state value ($l/a > 2$). There is a nonconvex region in the energy.
(2) With matrix constraint and therefore additional energy W_2, the nonconvex region of the total energy shrinks and finally disappears with the increase of the matrix constraint (i.e., the increase of $E^{(2)}/E^{(1)}$ or h/a, see Figs. 4 and 5).
(3) For all the cases with matrix constraint, the asymptotic linear part of W is proportional to the length of the inclusion. From the figures, this part of energy also increases with the matrix constraint (i.e., the increase of $E^{(2)}/E^{(1)}$ or h/a).

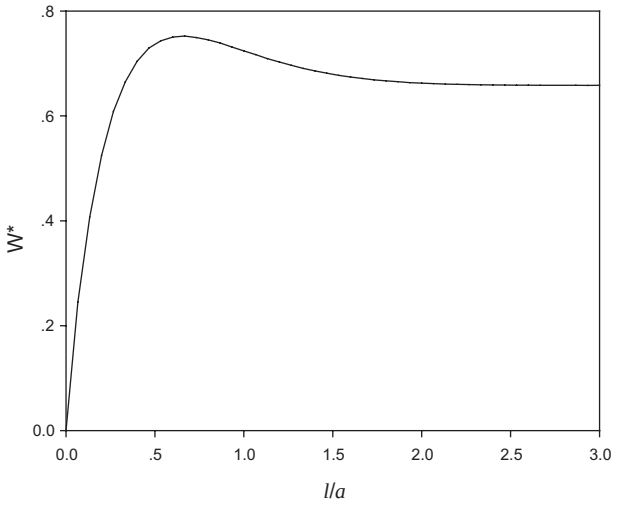

Fig. 3. Variation of the normalized elastic energy $W^*(= W/E^{(2)}a^3(\varepsilon_1^*)^2)$ of a constraint-free fiber versus the normalized inclusion length l/a.

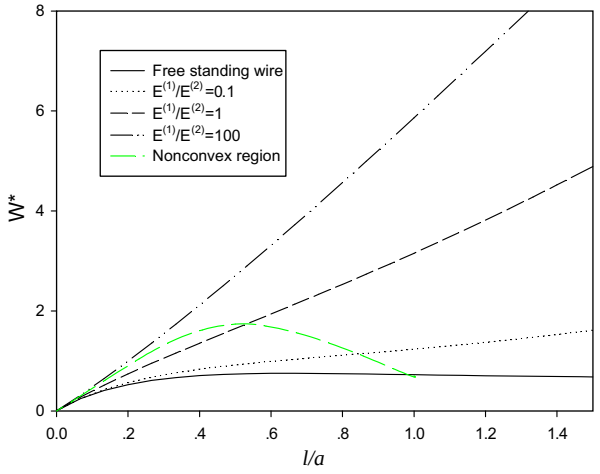

Fig. 4. Variation of the normalized elastic energy $W^*(= W/E^{(2)}a^3(\varepsilon_1^*)^2)$ of the system versus the normalized inclusion length l/a for different values of $E^{(1)}/E^{(2)}$ ($v^{(1)} = v^{(2)} = 0.3$, $h/a = 1$).

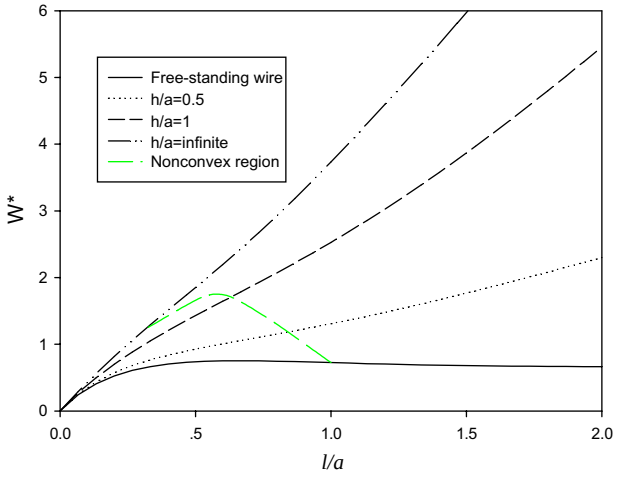

Fig. 5. Variation of the normalized elastic energy $W^*(= W/E^{(2)}a^3(\varepsilon_1^*)^2)$ of the system versus the normalized inclusion length l/a for different values of h/a ($v^{(1)} = v^{(2)} = 0.3$, $E^{(1)}/E^{(2)} = 5$).

4.2. Gibbs and Helmholtz free energy of the system

If the IFM system is further subjected to surface force—F_i, the Gibbs free energy of this IFM system is

$$\psi = \frac{1}{2}\int_{R^{(1)}} (\tilde{\sigma}_{ij}^{(1)} + \sigma_{ij}^{(1)})(\tilde{u}_{i,j}^{(1)} + u_{i,j}^{(1)})\,\mathrm{d}V + \frac{1}{2}\int_{R^{(2)}} (\tilde{\sigma}_{ij}^{(2)} + \sigma_{ij}^{(2)})(\tilde{u}_{i,j}^{(2)} + u_{i,j}^{(2)} - \varepsilon_{ij}^*)\,\mathrm{d}V$$
$$- \int_{\partial R^{(1)}} F_i(\tilde{u}_i^{(1)} + u_i^{(1)})\,\mathrm{d}S - \int_{\partial R^{(2)}} F_i(\tilde{u}_i^{(2)} + u_i^{(2)})\,\mathrm{d}S + \Delta W^{\mathrm{ch}} \tag{28}$$

where $\tilde{\sigma}_{ij}^{(i)}$ and $\tilde{u}_i^{(i)}$ are the corresponding stresses and displacements caused by the surface force in the absence of the inclusion. In order to see the physical meaning of ψ, Eq. (28) is decomposed into four terms:

$$\psi = \tilde{\psi} + \Delta W + W + \Delta W^{\mathrm{ch}} \tag{29}$$

where the first term,

$$\tilde{\psi} = \frac{1}{2}\int_{R^{(1)}} \tilde{\sigma}_{ij}^{(1)}\tilde{u}_{i,j}^{(1)}\,\mathrm{d}V + \frac{1}{2}\int_{R^{(2)}} \tilde{\sigma}_{ij}^{(2)}\tilde{u}_{i,j}^{(2)}\,\mathrm{d}V - \int_{\partial R^{(1)}} F_i\tilde{u}_i^{(1)}\,\mathrm{d}S - \int_{\partial R^{(2)}} F\tilde{u}_i^{(2)}\,\mathrm{d}S, \tag{30}$$

corresponds to the Gibbs free energy of the surface force in the absence of the inclusion. In the second term,

$$\Delta W = \frac{1}{2}\int_{R^{(1)}} \tilde{\sigma}_{ij}^{(1)}\varepsilon_{ij}^{(1)}\,\mathrm{d}V + \frac{1}{2}\int_{R^{(2)}} \tilde{\sigma}_{ij}^{(2)}\varepsilon_{ij}^{(2)}\,\mathrm{d}V - \frac{1}{2}\int_{\Omega} \tilde{\sigma}_{ij}^{(2)}\varepsilon_{ij}^{*}\,\mathrm{d}V - \int_{\partial R^{(1)}} F_i u_i^{(1)}\,\mathrm{d}S - \int_{\partial R^{(2)}} F_i u_i^{(2)}\,\mathrm{d}S \tag{31}$$

the stress and traction are associated with surface force and the strain and displacements are associated with the inclusion. Therefore, it is defined as the interaction energy. The third term, W, is the internal elastic energy induced by the inclusion alone (Eq. (21)). The last term, ΔW^{ch}, is the change of chemical free energy during transformation, which arises from the difference in Gibbs free energy between austenite and martensite. If the austenite phase is taken as the reference state, the total change in chemical free energy is

$$\Delta W^{\mathrm{ch}} = \int_{\Omega} \Delta\varphi(r)\,\mathrm{d}V = \Delta\varphi(T)\pi a^2 l \tag{32}$$

where $\Delta\varphi(T) = \varphi^{\mathrm{M}}(T) - \varphi^{\mathrm{A}}(T)$ is the chemical free energy density difference between the two phases. The change in chemical free energy density is only a function of the temperature. With a linear approximation around the equilibrium temperature T^0, the following form is commonly used (K is a constant determined from experiments)

$$\Delta\varphi(T) = \varphi^{\mathrm{M}}(T) - \varphi^{\mathrm{A}}(T) = K(T - T^0) \tag{33}$$

Therefore ΔW^{ch} is a function of T and the volume of the inclusion only.

Under external uniaxial tension the Gibbs free energy of the system can be expressed as the function of externally applied axial force F, temperature T and the inclusion length l as (taking $v^{(1)} = v^{(2)}$ for simplicity):

$$\begin{aligned}\psi = &-\frac{1}{2}\left\{\frac{(F^{(1)})^2}{\pi((a+h)^2 - a^2)E^{(1)}} + \frac{(F^{(2)})^2}{\pi a^2 E^{(2)}}\right\}L_0 - \frac{1}{2}(F^{(1)} + F^{(2)})u_0(l)\\ &+ \left(k(T - T_0)\pi a^2 - \frac{1}{2}F^{(2)}\varepsilon_z^*\right)l + W(l)\end{aligned} \tag{34}$$

In this equation, $F^{(1)}$ and $F^{(2)}$ are the traction act on the matrix and NiTi fiber. By the Saint–Venant theorem, they satisfy the following two equations

$$\frac{F^{(1)}}{\pi((a+h)^2 - a^2)E^{(1)}} = \frac{F^{(2)}}{\pi a^2 E^{(2)}}, \tag{35}$$

$$F^{(1)} + F^{(2)} = F, \tag{36}$$

except in the region near the end of the system. L_0 is the total length of IFM and $u_0(l)$ is the elongation of the IFM caused by the inclusion alone and is a function of the inclusion length l only. Assuming that the end surface does not deviate much from a plane, it can be approximated by

$$u_0(l) = u_Z^{(2)}|_{r=0,Z=L_0} \tag{37}$$

It must be pointed out that the above derivation of the Gibbs free energy of the IFM system is a kind of approximation since $u_0(l)$ and $W(l)$ are appropriated from the solution of the single inclusion problem of an infinite domain. However, because the dimensionless parameter $\frac{l}{L_0}$ is much less than unity, the difference between the solution of a bounded domain and that of the infinite domain is expected to be some order of $\frac{l}{L_0}$ and therefore is negligible.

Similarly, the Helmholtz free energy of the IFM system can be derived and expressed by the axial displacement u, temperature T and the inclusion length l as

$$\phi = \frac{1}{2}\frac{\{\pi a^2 E^{(2)} + \pi[(a+h)^2 - a^2]E^{(1)}\}(u - u_0(l))u}{L_0} + \left(k(T - T_0) - \frac{1}{2}\frac{u - u_0(l)}{L_0}E^{(2)}\varepsilon_z^*\right)\pi a^2 l + W(l) \tag{38}$$

It is seen that the martensite band length l appears naturally as an internal variable of the transformation process of single inclusion in the system.

4.3. Driving force and growth criteria of single band

Under slow loading rates, the whole system can be approximated as an isothermal one. The driving force for the interface motion can be obtained for force-controlled and displacement-controlled loading conditions respectively as:

$$\hat{f}(F,T,l) = -\left.\frac{\partial \psi}{\partial l}\right|_{F,T} = \frac{1}{2}(F^{(1)} + F^{(2)})\frac{\partial u_0}{\partial l} + \frac{1}{2}F^{(2)}\varepsilon_z^* - \frac{\partial W}{\partial l} - k(T - T_0)\pi a^2 \tag{39}$$

$$\begin{aligned}\hat{f}(u,T,l) &= -\left.\frac{\partial \phi}{\partial l}\right|_{u,T} \\ &= \frac{1}{2}\frac{\{\pi a^2 E^{(2)}(u - \varepsilon_z^* l) + \pi[(a+h)^2 - a^2]E^{(1)}u\}}{L_0}\frac{\partial u_0}{\partial l} + \frac{1}{2}\frac{E^{(2)}\pi a^2(u - u_0)\varepsilon_z^*}{L_0} - \frac{\partial W}{\partial l} - k(T - T_0)\pi a^2\end{aligned} \tag{40}$$

For the reversible transformation process (without energy dissipation), energy minimization gives (denoting time rate $\mathrm{d}(\ )/\mathrm{d}t$ by $(\dot{\bullet})$)

$$-\left.\dot{\psi}\right|_{F,T} = \hat{f}\dot{l} = 0 \tag{41}$$

$$-\left.\dot{\phi}\right|_{u,T} = \hat{f}\dot{l} = 0 \tag{42}$$

Then the criteria for both forward and reverse growths of the band can be immediately obtained in terms of force and displacement as

$$\begin{cases}\hat{f}(F,T,l) = 0 \\ \hat{f}(u,T,l) = 0\end{cases} \tag{43}$$

Substituting Eqs. (39) and (40) into Eq. (43), the explicit expression of *the growth criteria of a band* in terms of F and u are

$$\frac{1}{2}(F^{(1)} + F^{(2)})\frac{\partial u_0}{\partial l} + \frac{1}{2}F^{(2)}\varepsilon_z^* - \frac{\partial W}{\partial l} - k(T - T_0)\pi a^2 = 0 \tag{44}$$

$$\frac{\{\pi a^2 E^{(2)}(u-\varepsilon_z^* l)+\pi[(a+h)^2-a^2]E^{(1)}u\}}{2L_0}\frac{\partial u_0}{\partial l}+\frac{E^{(2)}\pi a^2(u-u_0)\varepsilon_z^*}{2L_0}-\frac{\partial W}{\partial l}-k(T-T_0)\pi a^2=0 \tag{45}$$

Eqs. (44) and (45) give the $F-l$, $u-l$, and $F-u$ relations during transformation as

$$F=F(l)=\frac{2\left[k(T-T_0)\pi a^2+\frac{\partial W}{\partial l}\right]}{\frac{\partial u_0}{\partial l}+M\varepsilon_z^*} \tag{46}$$

$$u=u(l)=\frac{\left[k(T-T_0)\pi a^2+\frac{\partial W}{\partial l}\right]2L_0+E^{(2)}\pi a^2\varepsilon_z^*\left(u_0+\frac{\partial u_0}{\partial l}l\right)}{\pi a^2E^{(2)}\left(\frac{\partial u_0}{\partial l}+\varepsilon_z^*\right)+\pi[(a+h)^2-a^2]E^{(1)}\frac{\partial u_0}{\partial l}} \tag{47}$$

$$F=F(u)=\frac{E^{(2)}\pi a^2\left(\frac{\partial u_0}{\partial l}+\varepsilon_z^*\right)+\pi[(a+h)^2-a^2]E^{(1)}\frac{\partial u_0}{\partial l}}{\left(\frac{\partial u_0}{\partial l}+M\varepsilon_z^*\right)L_0}u-\frac{E^{(2)}\pi a^2\varepsilon_z^*\left(u_0+l\frac{\partial u_0}{\partial l}\right)}{\left(\frac{\partial u_0}{\partial l}+M\varepsilon_z^*\right)L_0} \tag{48}$$

where

$$M=\frac{\pi a^2E^{(2)}}{\pi((a+h)^2-a^2)E^{(1)}+\pi a^2E^{(2)}}. \tag{49}$$

The nominal axial stress–stain relation of the system $\Sigma_{33}\sim E_{33}$ (with l as a monotonically increasing variable) can be obtained from Eqs. (48) and (49) as

$$\Sigma_{33}=\frac{E^{(2)}\left(\frac{\partial u_0}{\partial l}+\varepsilon_z^*\right)+E^{(1)}\frac{(a+h)^2-a^2}{\pi a^2}\frac{\partial u_0}{\partial l}}{\frac{\partial u_0}{\partial l}+M\varepsilon_z^*}\left(\frac{a}{a+h}\right)^2E_{33}-\frac{E^{(2)}\varepsilon_z^*\left(u_0+l\frac{\partial u_0}{\partial l}\right)}{\left(\frac{\partial u_0}{\partial l}+M\varepsilon_z^*\right)H_0}\left(\frac{a}{a+h}\right)^2 \tag{50}$$

In the above equations, $\frac{\partial u_0}{\partial l}$ can be calculated from Eqs. (37), (14) and (15) as

$$\frac{\partial u_0}{\partial l}=\varepsilon_z^*+\frac{(1+v^{(2)})}{E^{(2)}}\int_0^\infty[\rho_1^{(2)}(k)\chi_{21}^{(2)}(0)+\rho_3^{(2)}(k)\chi_{23}^{(2)}(0)]k^3\cos(kL_0)\,\mathrm{d}k \tag{51}$$

and $\frac{\partial W}{\partial l}$ can be calculated from Eqs. (22) and (19) as

$$\frac{\partial W}{\partial l}=\frac{\partial W_1}{\partial l}+\frac{\partial W_2}{\partial l} \tag{52}$$

$$\frac{\partial W_1}{\partial l}=\frac{\pi a^2}{1-v^{(2)}}E^{(2)}(\varepsilon_z^*)^2\left[1+\frac{1}{2}\int_0^\infty tG(t,v^{(2)})\sin\left(\frac{tl}{a}\right)\mathrm{d}t\right] \tag{53}$$

$$\begin{aligned}\frac{\partial W_2}{\partial l}=&-2\pi\varepsilon_1^*\int_0^\infty\{[2(1-2v^{(2)})\rho_1^{(2)}-\rho_3^{(2)}]kaI_1(ka)+k^2a^2\rho_1^{(2)}I_2(ka)\}k\sin(kl)\,\mathrm{d}k\\&-2\pi\varepsilon_2^*\int_0^\infty\{[-(4-2v^{(2)})\rho_1^{(2)}+\rho_3^{(2)}]kaI_1(ka)-k^2a^2\rho_1^{(2)}I_2(ka)\}k\sin(kl)\,\mathrm{d}k\end{aligned} \tag{54}$$

The above analysis can be extended to the irreversible process in real material by incorporating energy dissipation during phase transformation (see Sun and Zhong, 2000).

5. Evolution of the IFM system under uniaxial tension and deformation patterns of the fiber

5.1. Single martensite band growth

We first consider the transformation process by a single band nucleation and propagation. The external force F needed for the growth of the inclusion under different matrix constraint is calculated by Eq. (46). The variations of the scaled force with l/a for different matrix constraints are shown in Figs. 6 and 7. In Fig. 6, the matrix constraint is increased by increasing the Young's modulus of the matrix while holding the thickness of the matrix at $h/a = 1$; and in Fig. 7, the matrix constraint is increased by increasing the thickness of the matrix while holding the Young's modulus at $E^{(1)}/E^{(2)} = 5$. Other data needed in calculation are obtained from the experiments:

$T = 70$ °C, $k = 2.98 \times 10^{-4}$ GPa/°C, $E^{(2)} = 56.7$ GPa, $\varepsilon_z^* = 3.97\%$, $\varepsilon_r^* = -\frac{1}{2}\varepsilon_z^*$, $T_0 = 14.25$ °C, (Shaw and Kyriakides, 1995). In the calculation, because the initial band length l_0 should be of finite value, such as a typical grain size or microstructure length, we take $a = 0.1$ mm and $l_0 = \frac{a}{100}$ which is at the scale of the grain size of this material (the grain size of this material is about 1–10 μm). Features worth mentioning in these figures are:

(1) For single free fiber, the external force F decreases monotonically when the inclusion starts to grow from zero. After reaching its minimum value F increases with further growth of the inclusion and finally asymptotically reaches its steady-state value. As the matrix constraint increases, the decreasing part of F shrinks (see $E^{(1)}/E^{(2)} = 0.1, 0.5, 1$ in Fig. 6 and $h/a = 0.1, 0.5$ in Fig. 7) and eventually disappears (see Fig. 6 for $E^{(1)}/E^{(2)} =$ infinite and Fig. 7 for $h/a = 1$) and finally F increases monotonically to its steady-state value.
(2) With increase in the magnitude of the constraints, the steady-state value of F shifts up and finally exceeds its starting value at $l/a = 0$ (see $E^{(1)}/E^{(2)} = 1$ in Fig. 6 and $h/a = 0.5$ in Fig. 7).
(3) From the derivation of Section 4.3 we can see that at a given F, $\frac{\partial^2 \psi(l)}{\partial l^2} \sim \frac{\partial^2 W(l)}{\partial l^2} \sim \frac{\partial F(l)}{\partial l} < 0$, which imply the equilibrium inclusion length l is in the decreasing part of F and is in a nonconvex energy region. Therefore, the configuration is unstable under fixed applied load (soft device). In such case, for the given F,

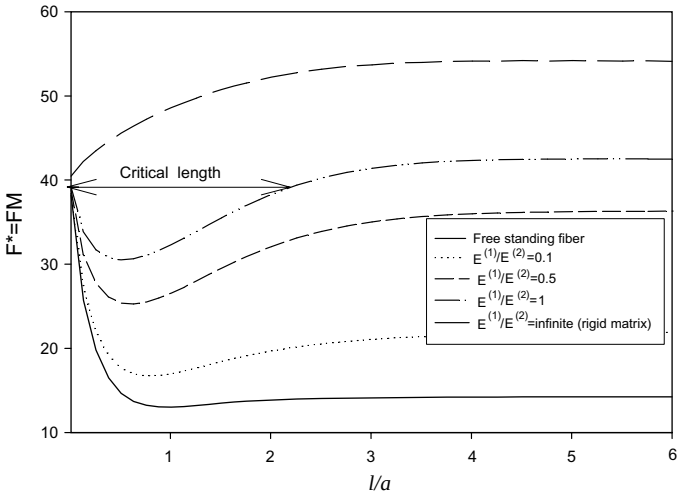

Fig. 6. Variation of the scaled force $F^*(= FM)$ of the system versus the normalized inclusion length l/a for different values of $E^{(1)}/E^{(2)}$ ($v^{(1)} = v^{(2)} = 0.3$, $h/a = 1$).

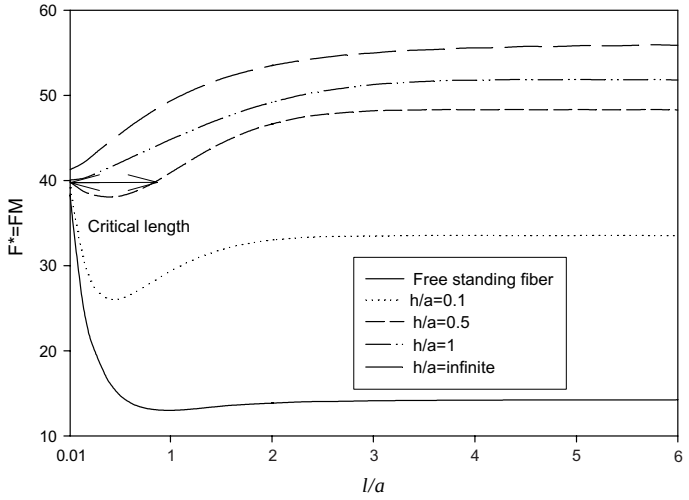

Fig. 7. Variation of the scaled force $F^*(=FM)$ of the system versus the normalized inclusion length l/a for different h/a ($v^{(1)} = v^{(2)} = 0.3$, $E^{(1)}/E^{(2)} = 5$).

if there are two equilibrium inclusion lengths, there will be a jump from the unstable length to the stable length. If there is only one equilibrium length (as in the case of free-standing fiber), the growth of the inclusion will be accelerated and the phase transformation will be accomplished under that dead load. The results in this section and in Section 5.3 again demonstrate that the stability of the equilibrium band length l depends on matrix constraint.

The above results imply that when the magnitude of the matrix constraint reaches a certain value, single band growth mode will not last long and a second martensite band (inclusion) will be nucleated and grow. With strong constraint, single band growth mode will be very difficult and some other deformation mode will appear. This will be discussed after the following introduction of nucleation and propagation criteria of a band.

5.2. Band nucleation criteria

By Eq. (46) the nominal stress of the system can be written as

$$\Sigma_{33} = \frac{F}{\pi(a+h)^2} = \frac{2\left[k(T-T_0)\pi a^2 + \frac{\partial W}{\partial l}\right]}{\left(\frac{\partial u_0}{\partial h} + M\varepsilon_z^*\right)\pi(a+h)^2} \tag{55}$$

Strictly speaking, band nucleation is a distinct instability process from band growth. For simplicity, we take the whole nucleation process of a band as a particular instance and equalize the nucleation stress to the initial growth stress (at the initial band length l_0). Therefore, *the nucleation criteria of a band* can be expressed as

$$\Sigma_{33}^{\mathrm{N}} = \left.\frac{F}{\pi(a+h)^2}\right|_{l=l_0} = \frac{2\left[k(T-T_0)\pi a^2 + \frac{\partial W}{\partial l}\big|_{l=l_0}\right]}{\left(\frac{\partial u_0}{\partial l}\big|_{l=l_0} + M\varepsilon_z^*\right)\pi(a+h)^2} \tag{56}$$

By the way, the stress for the steady-state growth of a single band is defined as

$$\Sigma_{33}^{\mathrm{SG}} = \left.\frac{F}{\pi(a+h)^2}\right|_{l=\infty} = \frac{2\left[k(T-T_0)\pi a^2 + \frac{\partial W}{\partial l}\big|_{l=\infty} + \pi a^2 D_0\right]}{\left(\frac{\partial u_0}{\partial l}\big|_{l=\infty} + M\varepsilon_z^*\right)\pi(a+h)^2} \tag{57}$$

Finally it is worth to mention that the nucleation always takes place from the boundary or from a point of inhomogeneity (defect). The analysis of the stress field as well as the band growth process can be applied to the cases, for example, the domain is semi-infinite and there is only one interface. In the following part, Eqs. (56) and (57) will be used as the criteria to analyze the transformation process in the system.

5.3. Transformation process of the fiber

From Figs. 6 and 7, the growth criteria (Eq. (46)), and the nucleation criteria (Eq. (56)), three fiber deformation patterns can be identified under uniaxial loading.

Type I: For fibers with weak constraint ($E^{(1)}/E^{(2)} = 0.1, 0.5$ in Fig. 6 and $h/a = 0.1$ in Fig. 7), after band nucleation the stress drops to a minimum and then increases asymptotically to the steady-state propagation value, which is lower than the nucleation stress. Therefore, after nucleation, the growth of single martensite band will continue until the fiber is fully transformed. This is called the single band propagation mode which is dominating under weak constraint.

Type II: For fibers with intermediate constraint ($E^{(1)}/E^{(2)} = 1$ in Fig. 6 and $h/a = 0.5$ in Fig. 7), the beginning of the stress–strain curve is like that of type I. After the stress gradually increases from its minimum, it will finally reach the value of the nucleation stress to form new band. Therefore further growth of the first inclusion will stop. In other words, after the inclusion reaches a certain critical length (in Fig. 6 for the case of $E^{(1)}/E^{(2)} = 1$, the critical length is about $2a$, and in Fig. 7 for the case where $h/a = 0.5$, it is about a) the growth will stop and a new band will nucleate at another site on the fiber. The new band will experience the same history as its predecessor until it reaches the critical length again. This procedure will be repeated. As a result, the nominal stress strain curve will show oscillation. This is called sequential band nucleation and propagation mode. (Note: the minimum distance between the sequential bands is determined by the distribution of matrix–fiber shear stress along the interface (see Fig. 8), which creates a compressive axial force in the fiber to prevent nucleation of new band in the close front of the existing interface). Moreover, for this characteristic distance, we temporally ignore the interaction between the inclusions for simplicity. It must be emphasized that the energy calculation of the successive nucleation process ahead of existing band is a good approximation only in the case where the bands are sufficiently apart from each other as briefly analyzed here and in Fig. 8. The excessive interaction energy due to the exponential boundary layers needs to be assessed when there is formation of many closely located interfaces. On the other hand, because of this reason, we expect that in the earlier stage of phase transition the formation of isolated inclusions is more advantage then the close ones and we can ignore the interaction energy between the inclusions for simplicity. For a complete simulation of the phase transition process, especially in the later stage when the bands start to merge, the interaction energy must be considered in the energetics of the IFM system.

Type III: For fibers with strong constraint ($E^{(1)}/E^{(2)} =$ infinite in Fig. 6, and $h/a = 1$ in Fig. 7), there is no drop of external stress after the nucleation. Instead, the stress increases monotonically. This implies that numerous bands will form in the fiber and the deformation of the fiber is macroscopically homogeneous.

Based on the above discussion, the following deformation patterns and the nominal stress and strain curves can be classified:

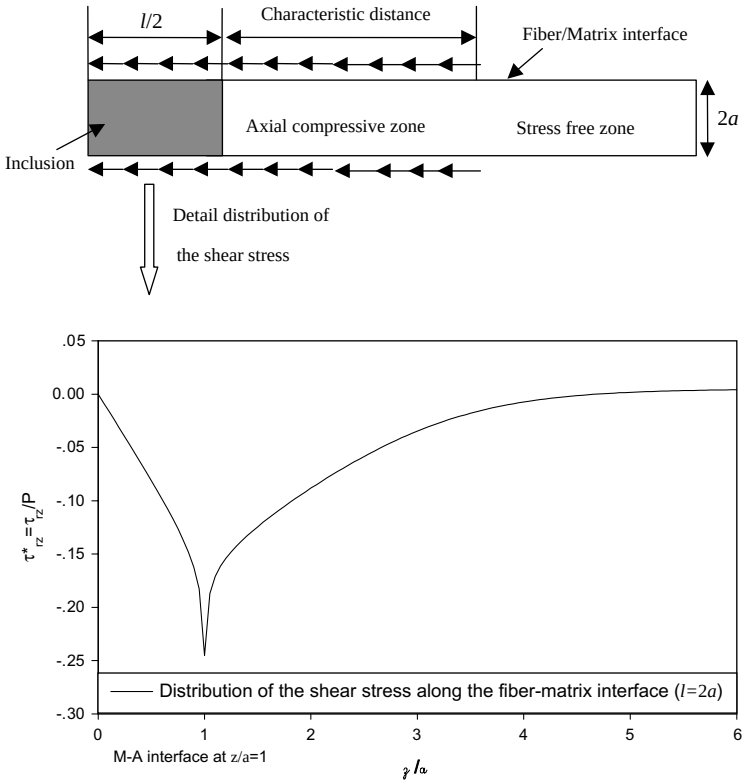

Fig. 8. Axial compressive zone along the fiber induced by the inclusion and the distribution of the normalized shear force $\tau^*_{rz} = \tau_{rz}/P$ (where $P = \frac{E^{(2)}}{1-\upsilon^{(2)}}\varepsilon_1^*$) along the fiber/matrix interface.

- For $\Sigma_{33}^{\mathrm{N}} > \Sigma_{33}^{\mathrm{SG}}$, the system favors single martensite nucleation and growth.
- For $\Sigma_{33}^{\mathrm{N}} < \Sigma_{33}^{\mathrm{SG}}$ and $\frac{\mathrm{d}\Sigma_{33}}{\mathrm{d}l}\big|_{l=l_0} < 0$, the system favors sequential bands nucleation and growth.
- For $\frac{\mathrm{d}\Sigma_{33}}{\mathrm{d}l}\big|_{l=l_0} > 0$, the system favors numerous bands formation and macroscopically the fiber tends to deform homogeneously.

Finally, from the above discussion on the types of deformation patterns and the corresponding conditions, it is seen that the range of parameters (like E, υ, h/a, etc) and the corresponding solutions (for example, multiple interfaces or two interfaces only) can be determined using numerical simulation. As implied by the results of Figs. 6 and 7, it is expected that solutions with one band (or two interfaces) will be the only local minima in the case of no matrix constraint, and on the contrary in the case of very stiff matrix or strong matrix constraint, relevant solutions will have very large number of interfaces.

6. Results of simulation and concluding remarks

6.1. Macroscopic response of the fiber matrix system

Based on the above analysis of deformation patterns and Eqs. (46)–(51), numerical simulation of the nominal stress and strain curves of the fiber matrix system under displacement control is performed and the

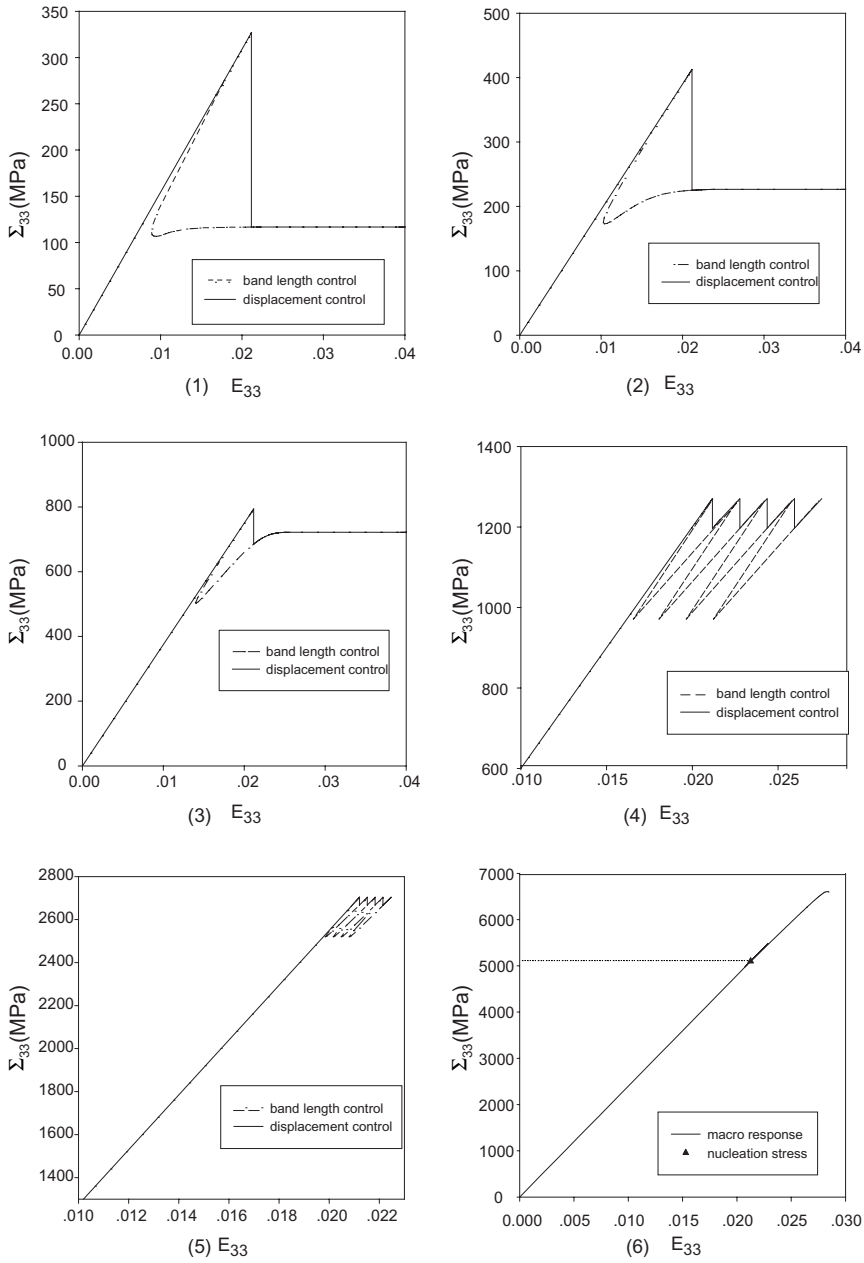

Fig. 9. Nominal stress–strain curves of the system for different values of $E^{(1)}/E^{(2)}$ (from (1) to (6), $E^{(1)}/E^{(2)} = 0.01, 0.1, 0.5, 1, 2.5, 5$) in case of $v^{(1)} = v^{(2)} = 0.3$, $h/a = 1$.

results are shown in Figs. 9 and 10. Depending on the matrix constraint (either relative Young's modulus or the relative thickness of the matrix), three different fiber deformation patterns appear.

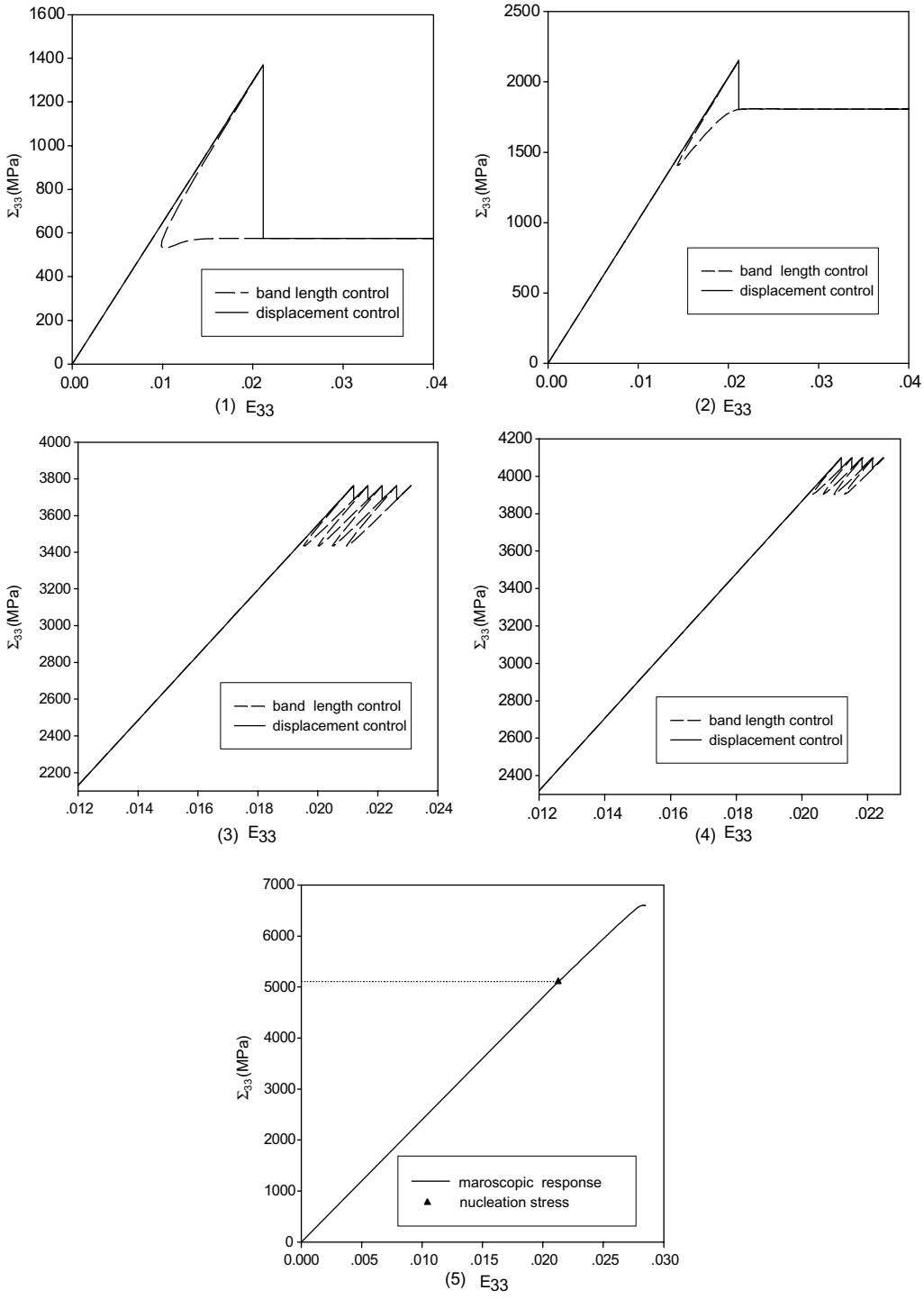

Fig. 10. Nominal stress–strain curves of the system for different value of h/a (from (1) to (5), $h/a = 0.01$, 0.1, 0.4, 0.5, 2) in case of $v^{(1)} = v^{(2)} = 0.3$, $E^{(1)}/E^{(2)} = 5$.

(1) Under weak matrix constraint, the fiber deforms in single band mode ($E^{(1)}/E^{(2)} = 0.01, 0.1, 0.5$ in Fig. 9 and $h/a = 0.01, 0.1$ in Fig. 10). Therefore there will be only one stress drop followed by a stress plateau in the nominal stress–strain curves of the system. As the constraint increases, the propagation stress will gradually approach the nucleation stress and eventually the deformation will switch to the sequential mode.
(2) Under intermediate matrix constraint ($E^{(1)}/E^{(2)} = 1, 1.5, 2.5$ in Fig. 9 and $h/a = 0.4, 0.5$ in Fig. 10), the fiber deforms by the sequential mode, hence the nominal stress–strain curves exhibit zigzag oscillations. Results also reveal that the greater the constraint, the smaller the oscillation magnitude. In Fig. 11, the variation of elastic strain energy W as define by Eq. (21) with the sequential band formation is plotted, in which each solid circle corresponds to the event that the former band stops growing while the new band emerges. The corresponding zigzag stress strain relation and the phase transformation process are also illustrated in Fig. 11(b) and (c). Since the nominal stress–stain relation is oscillatory, the energy will exhibit a wave-like landscape.
(3) Under strong matrix constraint ($E^{(1)}/E^{(2)} = 5$ in Fig. 9 and $h/a = 2$ in Fig. 10), numerous bands form along the fiber, which causes the fiber to deform homogeneously. As a result, the corresponding stress–strain curve of the system exhibits hardening.

To summarize, as the matrix constraint increases, the manner of fiber deformation changes from localized to homogeneous one. It is interesting to see that there exists similarity between the effect of the matrix constraint and the effect of A/M interface local heating due to latent heat (“loading rate” effect) on the transformation process and deformation mode of the NiTi fiber. At high loading rate, there is no enough time for the latent heat to convect into the environment; the local self-heating of the A–M interface makes it difficult for the existing band to grow. Therefore nucleation of a new band in other locations where the temperature is low will happen. Displacement-controlled uniaxial tension (see Shaw and Kyriakides, 1997; for details) revealed that as the loading rate increased, the deformation mode of a NiTi fiber switched from a single band to multiple bands and finally to numerous bands. The prediction we made on the effect of matrix constraint is also similar to the stress transfer observed during fiber fragmentation in composite materials (Cox, 1952), in the sense that both affect the growth ability of a localization zone.

6.2. Concluding remarks

Localization and propagation of martensite bands have been commonly observed in the tensile tests of a constraint-free superelastic NiTi wire and strip, and recently in small tubes (Li and Sun, 2002; Sun and Li, 2002). Though the mechanism for such deformation instability is still under investigation, it is generally believed that the cause of this instability lies upon the material’s intrinsic constitutive law during phase transformation. In this paper, we used an inclusion model to investigate the possible deformation patterns of the NiTi fiber subjected to different elastic matrix constraints. By examining the growth ability of a pre-existing inclusion, different deformation modes, which change with the matrix constraint, are identified.

In our treatment, the inclusion model and a nucleation criterion of a martensite band replace the nonlinear constitutive relations of the fiber. Here, band nucleation stress is postulated to be the initial growth stress of a band. The limitation of such an assumption can be reduced by a more rigorous bifurcation analysis of the governing equations that are derived from the free energy of the system (the nonconvex free energy of the NiTi fiber plus the convex free energy of the elastic matrix). Such analyses have been carried out for 2-D and 3-D nonconvex energy (Knowles and Sternberg, 1977; Triantafyllidis and Aifantis, 1986) and 1-D convex energy plus nonconvex energy (Truskinovsky and Zanzotto, 1995, 1996). 3-D bifurcation analysis of active fiber with matrix constraint might be the task of the future studies.

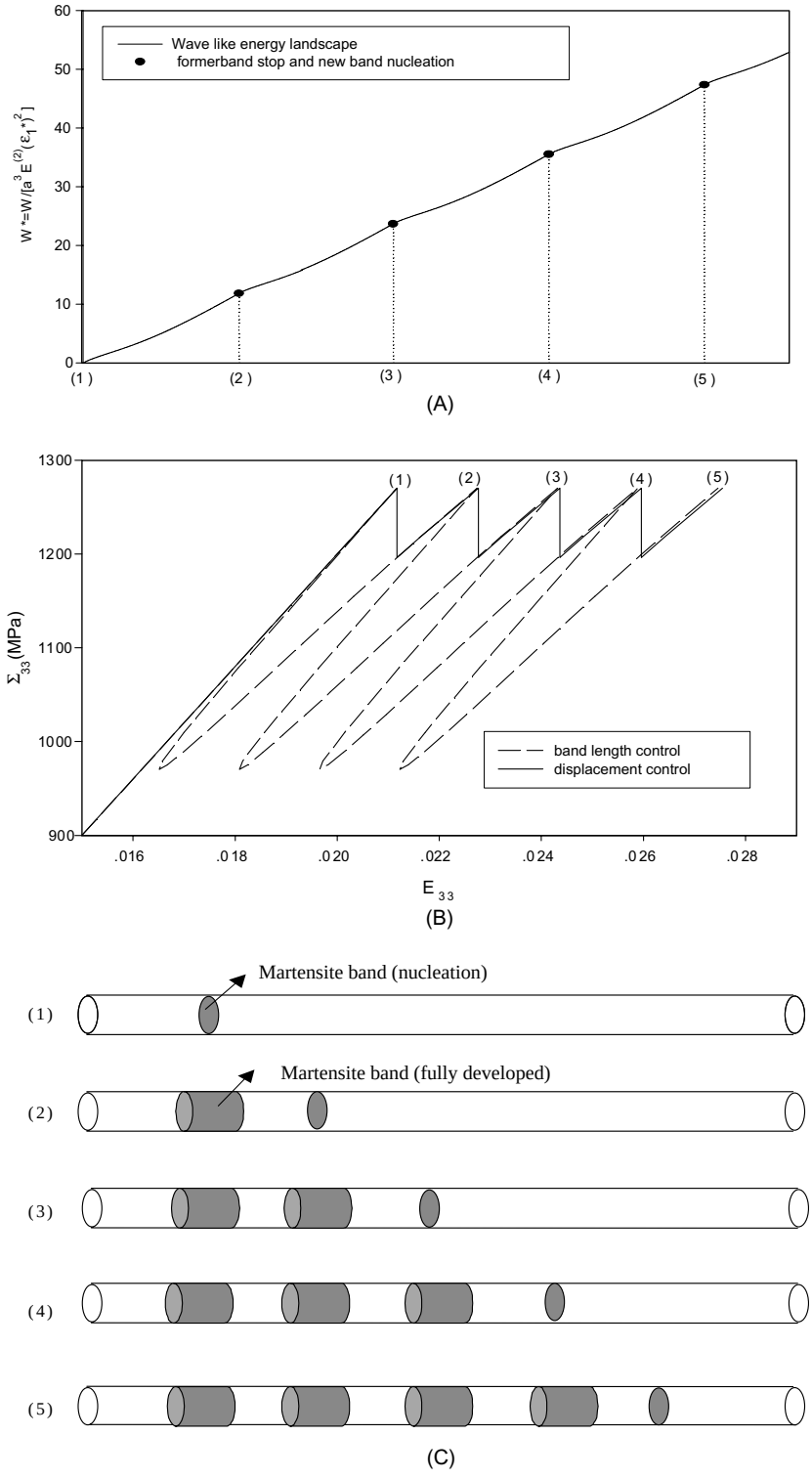

Fig. 11. (a) Wave-like energy landscape of sequential band nucleation and propagation; (b) corresponding zigzag stress strain curve; (c) corresponding sequential band nucleation and growth process in the fiber.

Acknowledgements

The authors are grateful for the financial supports from the Research Grants Council of The Hong Kong SAR (Project No. HKUST6037/98EHKUST6234/01E), the National Excellent Young Scholar Fund of China (Projects No. 10125209 and No. 19825107), and the Teaching and Research Award Fund for Outstanding Young Teachers in High Education Institutions of MOE, P.R.C.

Appendix A

$$M_{11}(kr) = -2(1-v)I_1(kr) - krI_0(kr) \quad M_{12}(kr) = 2(1-v)K_1(kr) - krK_0(kr)$$

$$M_{13}(kr) = I_1(kr) \quad M_{14}(kr) = -K_1(kr)$$

$$M_{21}(kr) = (1-2v)I_0(kr) + krI_1(kr) \quad M_{22}(kr) = (1-2v)K_0(kr) - krK_1(kr)$$

$$M_{23}(kr) = -I_0(kr) + \frac{I_1(kr)}{kr} \quad M_{24}(kr) = -K_0(kr) - \frac{K_1(kr)}{kr}$$

$$M_{31}(kr) = -(4-2v)I_0(kr) - krI_1(kr) \quad M_{32}(kr) = -(4-2v)K_0(kr) + krK_1(kr)$$

$$M_{33}(kr) = I_0(kr) \quad M_{34}(kr) = K_0(kr)$$

$$M_{41}(kr) = (1-2v)I_0(kr) \quad M_{42}(kr) = (1-2v)K_0(kr)$$

$$M_{43}(kr) = -\frac{I_1(kr)}{kr} \quad M_{44}(kr) = \frac{K_1(kr)}{kr}$$

$$\chi_{11}(kr) = krI_0(kr) \quad \chi_{12}(kr) = krK_0(kr)$$

$$\chi_{13}(kr) = -I_1(kr) \quad \chi_{14}(kr) = K_1(kr)$$

$$\chi_{21}(kr) = -4(1-v)I_0(kr) - krI_1(kr) \quad \chi_{22}(kr) = -4(1-v)K_0(kr) + krK_1(kr)$$

$$\chi_{23}(kr) = I_0(kr) \quad \chi_{24}(kr) = K_0(kr)$$

Appendix B

The equations for the determination of the unknown functions ρ_1^{I}, ρ_2^{I}, ρ_3^{I}, ρ_4^{I}, ρ_1^{II} and ρ_3^{II} are listed below:

$$\rho_1^{\mathrm{I}}(k)M_{11}[k(a+h)] + \rho_2^{\mathrm{I}}(k)M_{12}[k(a+h)] + \rho_3^{\mathrm{I}}(k)M_{13}[k(a+h)] + \rho_4^{\mathrm{I}}(k)M_{14}[k(a+h)] = 0 \tag{B.1}$$

$$\rho_1^{\mathrm{I}}(k)M_{21}[k(a+h)] + \rho_2^{\mathrm{I}}(k)M_{22}[k(a+h)] + \rho_3^{\mathrm{I}}(k)M_{23}[k(a+h)] + \rho_4^{\mathrm{I}}(k)M_{24}[k(a+h)] = 0 \tag{B.2}$$

$$\rho_1^{\mathrm{I}}(k)M_{11}(ka) + \rho_2^{\mathrm{I}}(k)M_{12}(ka) + \rho_3^{\mathrm{I}}(k)M_{13}(ka) + \rho_4^{\mathrm{I}}(k)M_{14}(ka) = \rho_1^{\mathrm{II}}(k)M_{11}(ka) + \rho_3^{\mathrm{II}}(k)M_{13}(ka) \tag{B.3}$$

$$\rho_1^{\mathrm{I}}(k)M_{21}(ka) + \rho_2^{\mathrm{I}}(k)M_{22}(ka) + \rho_3^{\mathrm{I}}(k)M_{23}(ka) + \rho_4^{\mathrm{I}}(k)M_{24}(ka) = \rho_1^{\mathrm{II}}(k)M_{21}(ka) + \rho_3^{\mathrm{II}}(k)M_{23}(ka) \tag{B.4}$$

$$\begin{aligned}&\frac{2(1+v^{(1)})}{E^{(1)}}[\rho_1^{\mathrm{I}}(k)\chi_{11}(ka) + \rho_2^{\mathrm{I}}(k)\chi_{12}(ka) + \rho_3^{\mathrm{I}}(k)\chi_{13}(ka) + \rho_4^{\mathrm{I}}(k)\chi_{14}(ka)]\\ &\quad = \frac{2(1+v^{(2)})}{E^{(2)}}\{[\rho_1^{\mathrm{II}}(k)\chi_{11}(ka) + \rho_3^{\mathrm{II}}(k)\chi_{13}(ka)] + [krI_0(ka) - \rho(k)I_1(ka)]f(k)\}\end{aligned} \tag{B.5}$$

$$\frac{2(1+v^{(1)})}{E^{(1)}}[\rho_1^{\mathrm{I}}(k)\chi_{21}(ka)+\rho_2^{\mathrm{I}}(k)\chi_{22}(ka)+\rho_3^{\mathrm{I}}(k)\chi_{23}(ka)+\rho_4^{\mathrm{I}}(k)\chi_{24}(ka)]$$
$$=\frac{2(1+v^{(2)})}{E^{(2)}}\{[\rho_1^{\mathrm{II}}(k)\chi_{21}(ka)+\rho_3^{\mathrm{II}}(k)\chi_{23}(ka)]+[(\rho(k)-4(1-v^{(2)}))I_0(ka)-kaI_1(ka)]f(k)\}$$
$$+\frac{2A}{\pi k^4} \tag{B.6}$$

References

Abeyaratne, R., Knowles, J.K., 1990. On the driving traction acting on a surface of strain discontinuity in a continuum. J. Mech. Phys. Solids 38, 345–360.

Abeyaratne, R., Knowles, J.K., 1993. A continuum model of thermoelastic solid capable of undergoing phase transitions. J. Mech. Phys. Solids 41, 541–571.

Cherkaoui, M., Sun, Q.P., Song, G.Q., 2000. Micromechanics modeling of composite with ductile matrix and shape memory alloy reinforcement. Int. J. Solids Struct. 37, 1577–1594.

Cox, H.L., 1952. The elasticity and strength of paper and other fibrous materials. Br. J. Appl. Phys. 3, 72–79.

Coleman, B.D., 1983. Necking and drawing in polymeric fibers under tension. Arch. Rat. Mech. Anal. 83, 115–137.

Duerig, T.W., Melton, K.N., 1989. Designing with the shape memory effect. In: Otsuka, K., Shimitsu, K. (Eds.), Proc. Shape Memory Materials, vol. 9, pp. 581–597. MRS International Meeting on Advanced Materials.

Ericken, J.L., 1975. Equilibrium of bars. J. Elasticity 5, 191–201.

Furuya, Y., 1996. Design and material evaluation of shape memory composites. J. Intell. Mater. Syst. Strut. 7, 321–330.

James, R.D., 1990. Microstructure of shape-memory and magnetostrictive materials. Appl. Mech. Rev. 43, 189–193.

Knowles, J.K., Sternberg, E., 1977. On the failure of ellipticity of the equations for finite elastostatics plane strain. Arch. Rat. Mech. Anal. 63, 321–336.

Li, Z.Q., Sun, Q.P., 2002. The initiation and growth of macroscopic martensite band in nano-grained NiTi microtube under tension. Int. J. Plasticity 18, 1481–1498.

Miyazaki, S., Imai, T., Otsuka, K., Suzuki, Y., 1982. Luders-like deformation observed in the transformation pseudoelasticity of a Ti–Ni alloy. Scr. Metall. 15, 853–856.

Mura, T., 1987. Micromechanics of Defects in Solids. Martinus Nijhoff, Dordrecht.

Roytburd, A.L., Slutsker, J., 1999a. Deformation of adaptive materials, Part I. Constrained deformation of polydomain crystal. J. Mech. Phys. Solids 47, 2299–2329.

Roytburd, A.L., Slutsker, J., 1999b. Deformation of adaptive materials, Part II. Adaptive composite. J. Mech. Phys. Solids 47, 2331–2349.

Roytburd, A.L., Slutsker, J., 2001. Deformation of adaptive materials, Part III. Deformation of crystals with polytwin product phases. J. Mech. Phys. Solids 49, 1795–1822.

Sun, Q.P., Zhong, Z., 2000. An inclusion theory for the propagation of martensite band in NiTi shape memory alloy fibers under tension. Int. J. Plasticity 16, 1169–1187.

Shaw, J.A., Kyriakides, S., 1995. Thermomechanical aspects of NiTi. J. Mech. Phys. Solids 43, 1243–1281.

Shaw, J.A., Kyriakides, S., 1997. On the nucleation and propagation of phase transformation fronts in a NiTi alloy. Acta Mater. 45 (2), 683–700.

Song, G.Q., Sun, Q.P., Cherkaoui, M., 1999. Role of microstructure in the thermo-mechanical behavior of SMA composites, ASME. J. Eng. Mater. Tech. 121 (1), 86–92.

Stupkiewicz, S., Petryk, H., 2002. Modelling of laminated microstructures in stress-induced martensitic transformations. J. Mech. Phys. Solids 50, 2303–2331.

Sun, Q.P., Li, Z.Q., 2002. Phase transformation in superelastic NiTi polycrystalline micro-tubes under tension and torsion—localization to homogeneous deformation. Int. J. Solids Struct. 39, 3797–3809.

Timoshenko, S., Goodier, J.N., 1951. Theory of Elasticity. McGraw-Hill Book Company, Inc., New York.

Triantafyllidis, N., Aifantis, E.C., 1986. A gradient approach to localization of deformation. I. Hyperelastic materials. J. Elasticity 16, 225–237.

Triantafyllidis, N., Bardenhagen, S., 1993. On higher order gradient continuum theories in 1-D nonlinear elasticity, derivation from and comparison to the corresponding discrete models. J. Elasticity 33, 259–293.

Truskinovsky, L., Zanzotto, G., 1995. Finite-scale microstructures and metastability in one-dimensional elasticity. Meccanica 30, 577–589.

Truskinovsky, L., Zanzotto, G., 1996. Ericksen's bar revisited: Energy wiggles. J. Mech. Phys. Solids 44, 1371–1408.
Tsai, H., Fan, X., 2002. Elastic deformations in shape memory alloy fibre reinforced composites. In: Sun, Q.P. (Ed.), Proceedings of the IUTAM Symposium on Mechanics of Martensite Phase Transformations in Solids. Kluwer Academic Publisher, pp. 139–146.
Zhong, Z., Sun, Q.P., Tong, P., 2000. On the axisymmetric deformation of a rod containing a single cylindrical inclusion. Int. J. Solids Struct. 37, 5943–5955.